A Facile Microwave Avenue to Electrochemiluminescent Two-Color Graphene Quantum Dots

Ling-Ling Li, Jing Ji, Rong Fei, Chong-Zhi Wang, Qian Lu, Jian-Rong Zhang, Li-Ping Jiang, and Jun-Jie Zhu**

With the assistance of microwave irradiation, greenish-yellow luminescent graphene quantum dots (gGQDs) with a quantum yield (QY) up to 11.7% are successfully prepared via cleaving graphene oxide (GO) under acid conditions. The cleaving and reduction processes are accomplished simultaneously using microwave treatment without additional reducing agent. When the gGQDs are further reduced with $NaBH_4$, bright blue luminescent graphene quantum dots (bGQDs) are obtained with a QY as high as 22.9%. Both GQDs show well-known excitation-dependent PL behavior, which could be ascribed to the transition from the lowest unoccupied molecular orbital (LUMO) to the highest occupied molecular orbital (HOMO) with a carbene-like triplet ground state. Electrochemiluminescence (ECL) is observed from the graphene quantum dots for the first time, suggesting promising applications in ECL biosensing and imaging. The ECL mechanism is investigated in detail. Furthermore, a novel sensor for Cd^{2+} is proposed based on Cd^{2+} induced ECL quenching with cysteine (Cys) as the masking agent.

1. Introduction

Graphene has triggered a gold rush to develop its applications in various fields, and increasing efforts have been made to exploit the fluorescence properties of graphene-based materials.[1–6] Nevertheless, as graphene is a zero-bandgap material, the possibility of observing its luminescence is almost impossible.[1,7] Thus the manipulation of the graphene bandgap by various means has stirred great interest, including opening the bandgap of graphene through doping,[4] manipulating graphene oxide (GO) through partial reduction and surface passivation,[8,9] and cleaving graphene-based materials into nanoscale graphene quantum dots (GQDs) to induce photoluminescence (PL).[2,3,5,6]

Theoretical and experimental studies have shown that GQDs (less than 10 nm in size) possess more pronounced edge effect and stronger quantum confinement effect than graphene nanoribbons.[3,6] This property can be expected to induce interesting phenomena that may be difficult to be observed in other semiconductors.[10] The GQDs have some fascinating merits, including low cytotoxicity, excellent solubility, stable photoluminescence, good biocompatibility, high specific surface area, high mobility and tunable band gap, thus making them promising in photovoltaic devices, biosening and imaging.[2,6]

However, the synthesis of GQDs is still at an early stage. Most reported approaches for GQDs can be classified into two main groups: bottom-up[10,11] and top-down,[2,3,5,6] wherein the former is limited by complex processes, severe synthetic conditions and difficulty for mass production. The top-down approaches consist of the decomposition of suitable precursors. The oxygen-containing functional groups could create defects on GO sheets and serve as chemically reactive sites that allow GO to be cleaved into smaller sheets,[7] that is the basis of most top-down strategies for GQDs. Besides, the epoxy and carboxylic groups on GO usually result in non-radiative recombination of localized electron–hole pairs.[9] Consequently, the subsequent reduction process after the cleaving of GO is necessary.[3,5] Most GQDs reported at present are partially reduced.[2,3,6] Nevertheless, these GQDs are facing more or less problems demanding urgent solution. For example, the hydrothermal cleaving routes involve separate cleaving and reduction processes, which is time consuming (up to three days), and the corresponding quantum yields (QYs) of GQDs are very low (<8%).[3,5] Strongly fluorescent GQDs have also been prepared by one-step solvothermal method with QY as high as 11.4%.[6] However, this approach may be limited by low product yield (1.6%) and the use of organic solvent. Thus the facile aqueous synthetic route to high-quality GQDs in large scale is still imminently desired.

Microwave-assisted technique has been widely applied to materials synthesis. Microwave irradiation can offer rapid and uniform heating for the reaction medium, and thus reaction time is dramatically shortened, product yields and purities was greatly improved.[12–14] Moreover, microwave assisted reduction of GO has been reported.[15,16] On the basis of the versatility of microwave, it is potentially promising to explore the rapid one-step synthesis of luminescent GQDs.

Electrochemiluminescence (ECL) of QDs, since reported by Ding and Bard in 2002,[17] has been widely used in fundamental

Dr. L.-L. Li, J. Ji, R. Fei, C.-Z. Wang, Q. Lu, Prof. J.-R. Zhang, Dr. L-P. Jiang, Prof. J.-J. Zhu
State Key Laboratory of Analytical Chemistry for Life Science, School of Chemistry and Chemical Engineering, Nanjing University
Nanjing, 210093, P. R. China
E-mail: Jianglp@nju.edu.cn; jjzhu@nju.edu.cn

DOI: 10.1002/adfm.201200166

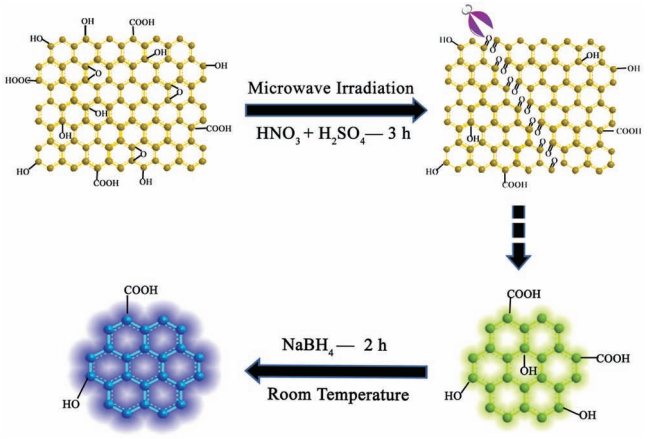

Scheme 1. Schematic representation of the preparation route for gGQDs and bGQDs.

study and analytical applications.[18–20] However, the inherent toxicity of Cd-based semiconductors used in most ECL studies may raise serious health and environmental problem. Therefore, the search for benign nanomaterials with good ECL activities has become an urgent challenge. In the case of GQDs, due to their low cytotoxicity and attractive biocompatibility, it is of considerable interest to study their ECL behaviors. Up to now, no references have been found involving the ECL research of GQDs.

Herein, we report a facile one-pot microwave-assisted approach for the preparation of stabilizer-free greenish yellow-luminescent GQDs (gGQDs) from GO nanosheets under acid conditions (3.2 M HNO_3 and 0.9 M H_2SO_4) within 3 h. Brightly blue-luminescent GQDs (bGQDs) were also obtained via moderately reducing GQDs with $NaBH_4$ within 2 h. The PL QYs of gGQDs and bGQDs were as high as 11.7% and 22.9%, respectively (Table S1). The optical properties of the gGQDs and bGQDs have been studied and proposed to originate from transition between LUMO and HOMO. Furthermore, ECL behaviors of the as-prepared gGQDs and bGQDs were observed with $K_2S_2O_8$ as coreactant, and the mechanism has been discussed in detail. A novel ECL sensor for Cd^{2+} was proposed based on the intense ECL of gGQDs. The GQDs could become a promising alternative material for ECL investigations and applications. **Scheme 1** outlines the preparation route to gGQDs and bGQDs, wherein the cleaving mechanism is described. Briefly, initiated by the acid oxidation of epoxy groups, it is prone to form a mixed line on the carbon lattice composed of fewer epoxy groups and more carbonyl groups, making the graphitic domains fragile and readily attacked[3,21].

2. Results and Discussion

2.1. Structural Characterization

The color of GO-HNO_3-H_2SO_4 mixture changed from yellow to brownish-black after microwave treatment (Figure S1, Supporting Information). It is speculated that GO was somewhat reduced during the cleaving process. This speculation is further proved by Fourier transform infrared (FTIR) and X-ray photoelectron spectroscopy (XPS) spectra (**Figure 1**). In the FTIR spectra, the gGQDs and bGQDs only showed C–O (alkoxy) stretching peak at 1112 cm^{-1} and C–O (carboxy) deformation peak at 1389 cm^{-1}, and the C–O (epoxy) stretching vibration peak at 1260 cm^{-1} disappeared entirely,[16,22] which is consistent with previous reports that epoxy groups could serve as chemically reactive sites for the rupture of the underlying C-C bonds.[3] Furthermore, the XPS of the gGQDs and bGQDs (Figure 1c,d) showed three kinds of carbon:[23–25] graphitic carbon (C=C and C–C), oxygenated carbon and nitrous carbon. The nitrogen originated from HNO_3 oxidation which induced doping of nitrogen into GQDs through a small extent of nitration.[26] The percentages of oxygen/nitrogen-bonded carbon in gGQDs and bGQDs decreased progressively in comparison with GO (**Table 1**), indicating that reduction occurred during the microwave treatment.

The reduction effect was also proved with the zeta potential as shown in Table 1. The quantum dots solutions remained homogeneous even after 4 months at room temperature without any perceptible changes. The time evolution of the PL spectra (Figure S4a, Supporting Information) showed that the peak value of gGQDs kept constant regardless of reaction time, thus the cleaving and reduction might occur simultaneously. As a result, microwave irradiation integrated the cleaving and reduction steps into facile one step and finally simplified the synthetic process and shortened the reaction time.

Figure 2 shows the high-resolution transmission electron microscope (HRTEM) and atomic force microscopy (AFM) images of GO and the both GQDs. The diameters of gGQDs were mainly distributed in the range of 2–7 nm with average diameter of 4.5 nm (Figure 2a), which is similar to previous reports.[2,6] Inset in Figure 2a is the representative image of individual gGQDs, indicating high crystallinity of the gGQDs, with a lattice parameter of 0.345 nm, which is consist with previous report.[27] The topographic heights of gGQDs were mostly between 0.5 and 2 nm with average height of 1.2 nm (Figure 2e), suggesting that most of gGQDs were single layered or bilayered.[6] The dimensions and height of bGQDs showed no perceptible change (Figure 2b,f), indicating that the PL blue-shift of bGQDs could be attributed to their structural change after reduction rather than their dimension variation.

2.2. Optical Characterization

To further explore the optical properties of the gGQDs and bGQDs, PL and UV-vis absorption spectra were studied (**Figure 3**). For the UV-vis absorption of gGQDs, a typical absorption peak at ca. 265 nm can be observed, and the strong background absorption below 300 nm was assigned to the π–π^* transition of aromatic sp^2 domains.[3,28] Similar to previous reports,[2,3,5,6] the gGQDs also exhibited an excitation-dependent PL behavior. With the excitation wavelength changed from 300 to 540 nm, the PL peak shifted to longer wavelengths with the strongest peak at 500 nm when excited at 260 nm and 340 nm. The PL excitation (PLE) spectrum recorded with the strongest luminescence (500 nm) showed two distinct peaks at 265 nm (4.68 eV) and 346 nm (3.58 eV) (Figure 3d).

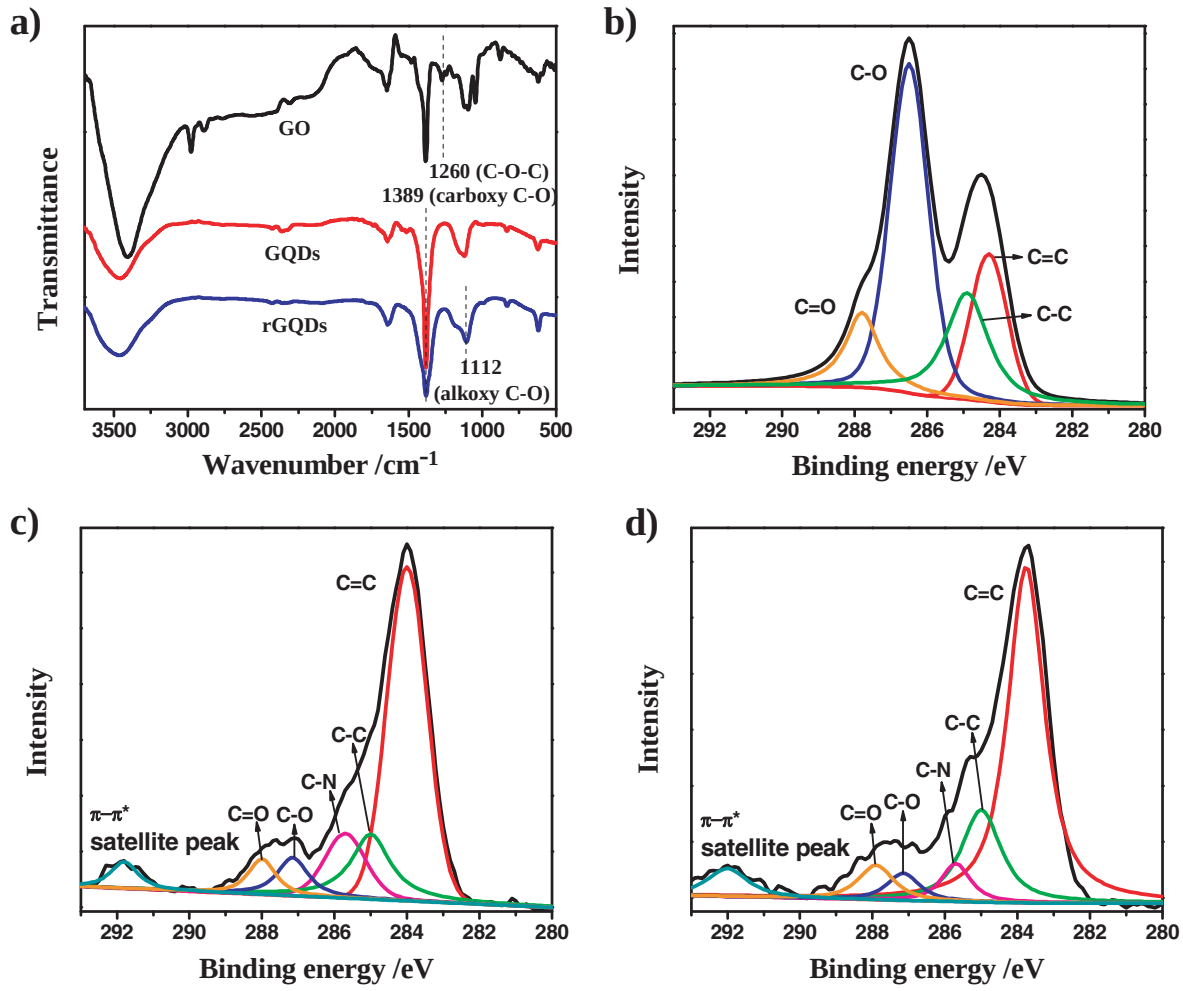

Figure 1. a) FTIR spectra of GO, gGQDs, and bGQDs. XPS C1s analysis of b) GO, c) gGQDs, and d) bGQDs.

The 265-nm PLE peak corresponded to the 265-nm absorption band of gGQDs, whereas the corresponding absorption band of the 346-nm PLE peak was negligible.

The bGQDs showed a dramatic increase in the PL intensities, accompanied with obvious blue-shift of the emission peak (Figure 3b,c). The emission spectra of the bGQDs also showed a similar excitation-dependent feature with the strongest peak (450 nm) excited at 260 nm and 340 nm. Nevertheless, the corresponding PLE spectrum showed tiny difference, a blue-shifted peak at 336 nm (3.69 eV) and a stronger one at 265 nm (4.68 eV) could be observed. The gGQDs and bGQDs aqueous solutions exhibited greenish yellow and blue fluorescence excited by 365 nm lamp (Figure 3a,b, inset). The proposed synthetic approach was compared with ordinary hydrothermal method at 95 °C for 24 h (Figure 3c), the obvious merit of microwave irradiation emerged thereby.

Table 1. XPS analysis and zeta potentials of GO, gGQDs, and bGQDs.

Sample	C=C and C–C [%]	Oxygenated C and Nitrous C [%]	Zeta Potential [mV]
GO	40.30	59.70[a)]	–58
gGQDs	74.30	25.70[b)]	–20
bGQDs	83.14	16.86[b)]	–8

[a)]Only the oxygen-containing carbon (C–OH, C=O, C–O, O–C=O); [b)]Oxygenated C and Nitrous C.

According to previous reports,[3,5] the fluorescence of GQDs may originate from emissive free zigzag sites with a carbene-like triplet ground state described as $\sigma^1 \pi^1$. The carbene ground-state multiplicity is related to energy difference (δE) between σ and π orbitals which should be below 1.5 eV determined by Hoffmann. Herein, the two electronic transitions of 265 nm (4.68 eV) and 346 nm (3.58 eV) in the PLE spectra can be regarded as transitions from σ and π orbitals, namely highest occupied molecular orbital (HOMO) to the lowest unoccupied molecular orbital (LUMO).[3] The δE of the gGQDs was thus determined to be 1.1 eV, within the required value (<1.5 eV) for triple carbenes. The δE of the bGQDs was 0.99 eV (<1.5 eV). Thus, the PL spectra of both GQDs here are related to transition

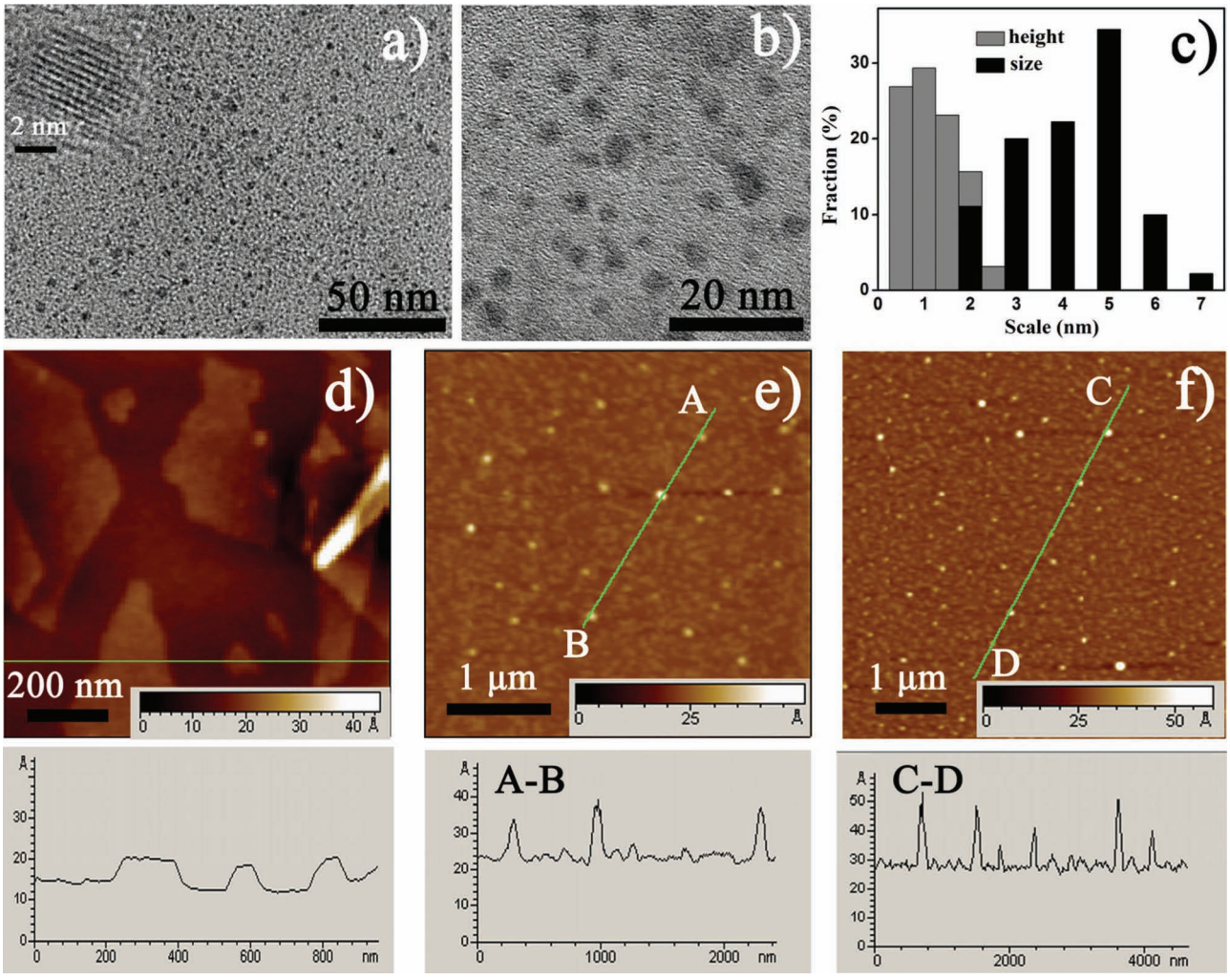

Figure 2. HRTEM images of a) gGQDs and b) bGQDs. The inset of (a) is a representative image of individual gGQDs. c) Size and height distributions of gGQDs. d–f) AFM images and their corresponding height profiles of GO, gGQDs, and bGQDs, respectively.

from the LUMO to the HOMO, and the energy difference between gGQDs and bGQDs via moderate reduction may contribute to the blue-shift of PL. Moreover, the emission intensity of bGQDs depended upon the degree of reduction, namely reaction temperature and time, and higher degree of reduction could result in eventual quenching of the PL signal without any peak shift (Figure S4b). The result is consistent with previous report, which is ascribed to the concentration change of small sp^2 carbon clusters with higher band gap embedded in sp^3 matrix during reduction.[1]

2.3. ECL Investigations

Furthermore, ECL behaviors of the obtained gGQDs and bGQDs were studied in 0.05 M, pH 7.4 Tris-HCl buffer solution (TBS) with 0.1 M $K_2S_2O_8$ as coreactant. As shown in **Figure 4**a, when the potential was cycled negatively between 0 and –1.6 V, gGQDs showed an intense ECL emission at –1.45 V, with an onset potential at about –0.9 V, which was about 9 times higher than background signal. No obvious ECL was observed in the absence of $K_2S_2O_8$, indicating the important role of $K_2S_2O_8$ as coreactant. Meanwhile, the ECL behavior of GO was also investigated. As shown in Figure S5 (Supporting Information), in comparision with gGQDs, the same concentration of GO had no obvious ECL signal, ruling out the interference from the starting materials in the ECL process of GQDs. Moreover, the cyclic voltammograms (CVs) in Figure 4a revealed that, apart from the reduction peak of $S_2O_8^{2-}$ around –0.8 V in the CVs of the background and gGQDs, a small peak at –1.36 V appeared. This peak was closed to the above-mentioned ECL peak (–1.45 V) and thus could be assigned to the reduction peak of gGQDs.

Figure 4b shows the ECL spectrum of gGQDs with the maximum wavelength at 512 nm, which is tinily red-shifted (12 nm) compared with the gGQDs PL spectrum excited at 340 nm, suggesting the negligible surface defect of the gGQDs.[29] An attractive merit of gGQDs in ECL study is the well-defined ECL

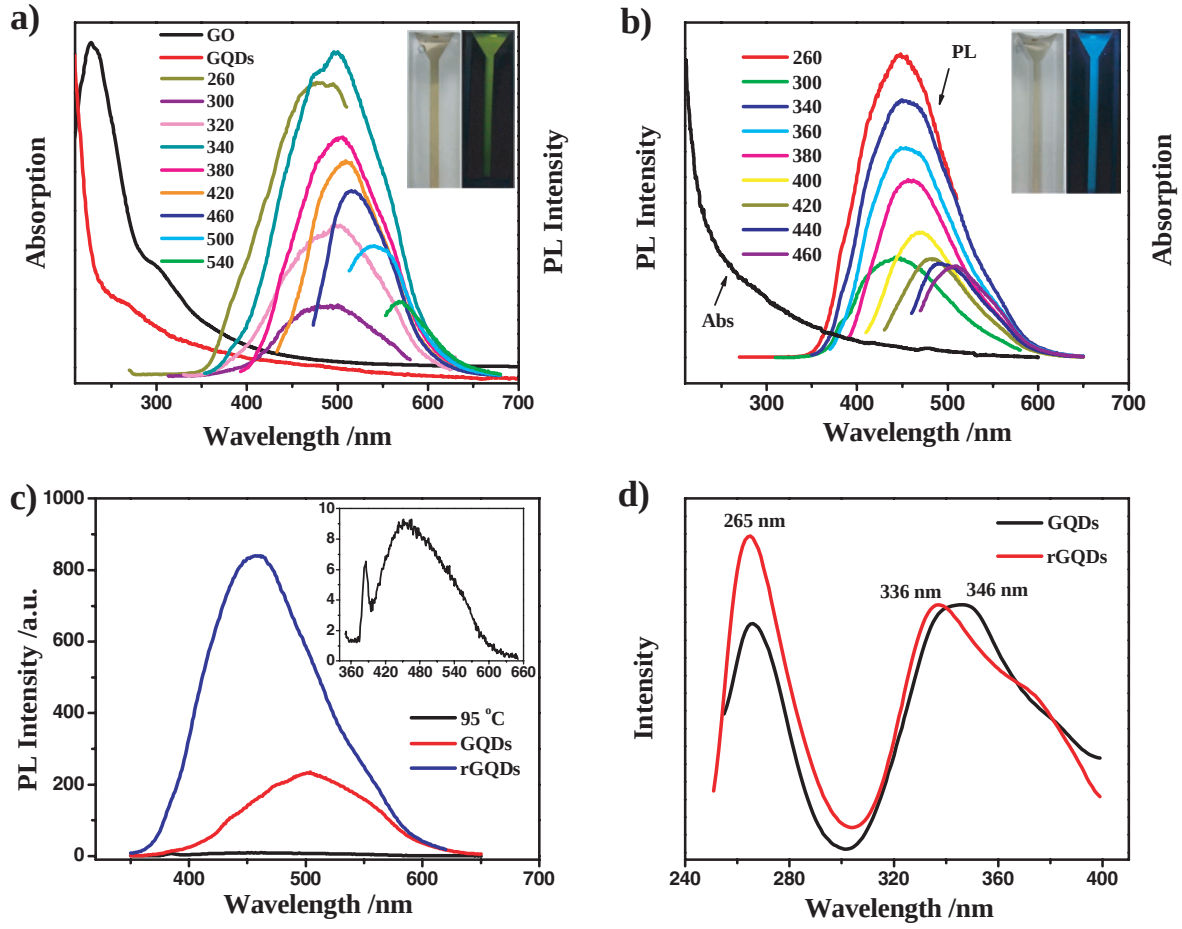

Figure 3. a) UV-vis absorption (Abs, red) and PL spectra of the gGQDs at different excitation wavelengths; UV-vis absorption (Abs, black) spectrum of GO. b) Absorption and PL spectra of the bGQDs at different excitation wavelengths. Insets in (a,b): photographs of the gGQDs and bGQDs aqueous solution taken under visible light and 365 nm UV light. c) PL spectra of gGQDs and bGQDs prepared through microwave and GQDs through hydrothermal route (at 95 °C) excited at 340 nm. d) PLE spectra of gGQDs (500 nm) and bGQDs (450 nm).

peak at relatively positive potential in comparison with previously reported carbon and silicon nanocrystals (NCs).[17,19,30,31] Apart from the difference in energy gap, this merit might also profit from high content of sp^2 carbon domains in gGQDs inherited from graphene, which could accelerate electron transport during ECL process.

Different from the stronger PL emission of bGQDs, the ECL intensity of bGQDs was weaker than gGQDs, and the emission peak negatively shifted to –1.72 V (Figure 4c), probably because the bGQDs emerged higher band gap and reduction resistance than gGQDs.

ECL measurements of the gGQDs upon continuous cyclic scans in TBS showed constant signals with relative standard deviation (RSD) of 1.3% (**Figure 5**), indicating the excellent stability.

Obviously, the ECL behaviors of both GQDs are similar to that of other QDs, such as CdSe,[20] carbon NCs,[19] and Si NCs.[17] Consequently, the ECL mechanism of the GQDs was proposed as follows: firstly, strongly oxidizing $SO_4^{\bullet-}$ radicals and $GQDs^{\bullet-}$ radicals were produced by electrochemical reduction of $S_2O_8^{2-}$ and GQDs, respectively. Then, $SO_4^{\bullet-}$ radicals could react with $GQDs^{\bullet-}$ via electron-transfer annihilation, producing an excited state (GQDs*) that finally emitted light. The possible ECL mechanisms are described in **Figure 6** with the following equations:

$$GQDs + ne^- \rightarrow nGQDs^{\bullet-}$$

$$S_2O_8^{2-} + e^- \rightarrow S_2O_8^{\bullet 2-}$$

$$S_2O_8^{\bullet 2-} \rightarrow SO_4^{2-} + SO_4^{\bullet-}$$

$$GQDs^{\bullet-} + SO_4^{\bullet-} \rightarrow GQDs^* + SO_4^{2-}$$

$$GQDs^* \rightarrow GQDs + hv$$

2.4. Detection of Cd^{2+}

On the basis of their intense ECL, gGQDs were also applied in the determination of Cd^{2+}. Cd^{2+} is generally known as a highly toxic metal ion that acts as a carcinogen in mammals, it can accumulate in organs such as the kidney, thyroid gland, lung, liver, spleen, and the immune system.[32] Therefore, the accurate determination of Cd^{2+} is of great importance.

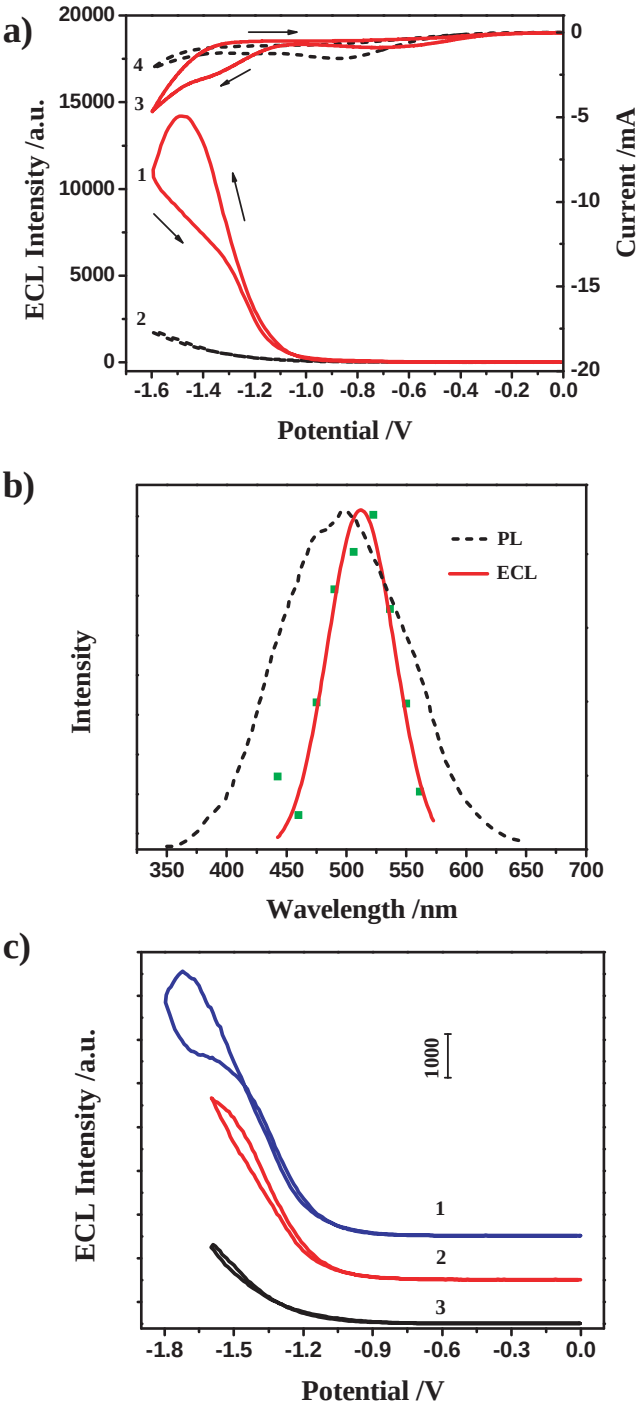

Figure 4. a) ECL-potential curves and cyclic voltammograms (CVs) of the gGQDs (1,3) and background (2,4) with concentration of 20 ppm in 0.05 M Tris-HCl (pH 7.4) buffer solution containing 0.1 M $K_2S_2O_8$. Scan rate: 100 mV s^{-1}. b) PL (λ_{ex} = 340 nm) and ECL spectra for the gGQDs-$K_2S_2O_8$ system. c) ECL-potential curves of the background (1) and bGQDs (20 ppm) (2,3) in 0.05 M Tris-HCl (pH 7.4) buffer solution containing 0.1 M $K_2S_2O_8$.

As depicted by the black line in **Figure 7**b, when various metal ions (20 μM) were added into the pH 7.4 TBS (0.05 M) with 0.1 M $K_2S_2O_8$ and 20 ppm gGQDs, six kinds of ions

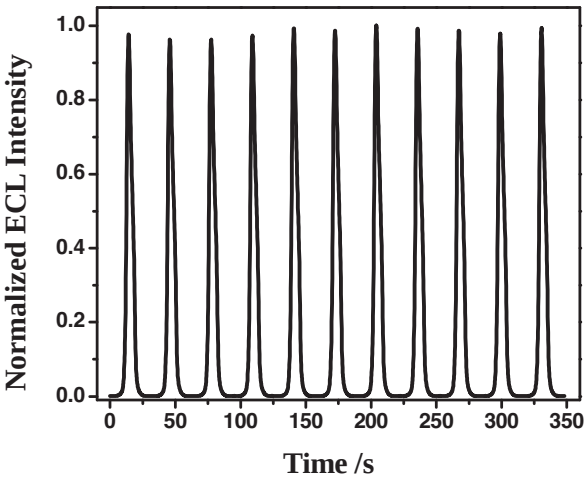

Figure 5. ECL responses of gGQDs-$S_2O_8^{2-}$ system obtained during a continuous potential scan between −1.6 and 0 V.

including Ni^{2+}, Pb^{2+}, Cu^{2+}, Co^{2+}, Fe^{2+} and Cd^{2+} could quench the ECL, while other ions had no obvious effect on ECL emission. It is noteworthy that 20 μM Cd^{2+} could lead to almost 92% quenching of gGQDs ECL (curve 2 in Figure 7a,b). However, it could not cause obvious ECL decrease (just about 4.9%) with blank electrolyte in the absence of gGQDs (Figure S6, Supporting Information). Therefore, the ECL quenching could be induced by the interaction between metal ions and GQDs.

Furthermore, it was found that when a certain amount of ethylenediaminetetraacetic acid (EDTA) was added, the quenched ECL of gGQDs could be almost completely recovered (Figure 7b, grey line). Because EDTA is a strong metal ion chelator, it can bind metal ions through coordination with its acidic and amino functional groups. As verified by FTIR, XPS and zeta potential, the obtained gGQDs were covalently decorated with oxygen-containing functional groups, such as hydroxyl and carboxyl groups, as well as doped nitrogen. All these functional groups were reported to have complexation ability with metal ions.[32–36] Therefore, these functional groups of gGQDs could serve as effective coordination groups for metal ions and thereby induced the aggregation of gGQDs, leading to the

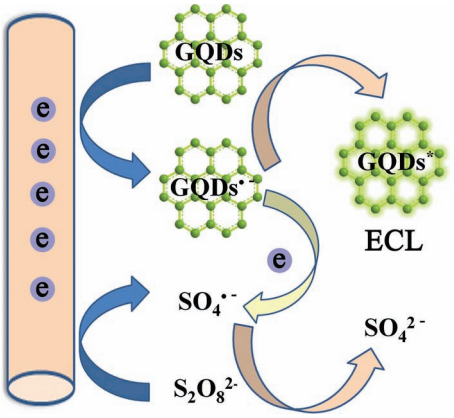

Figure 6. Schematic illustration of the ECL mechanism of GQDs.

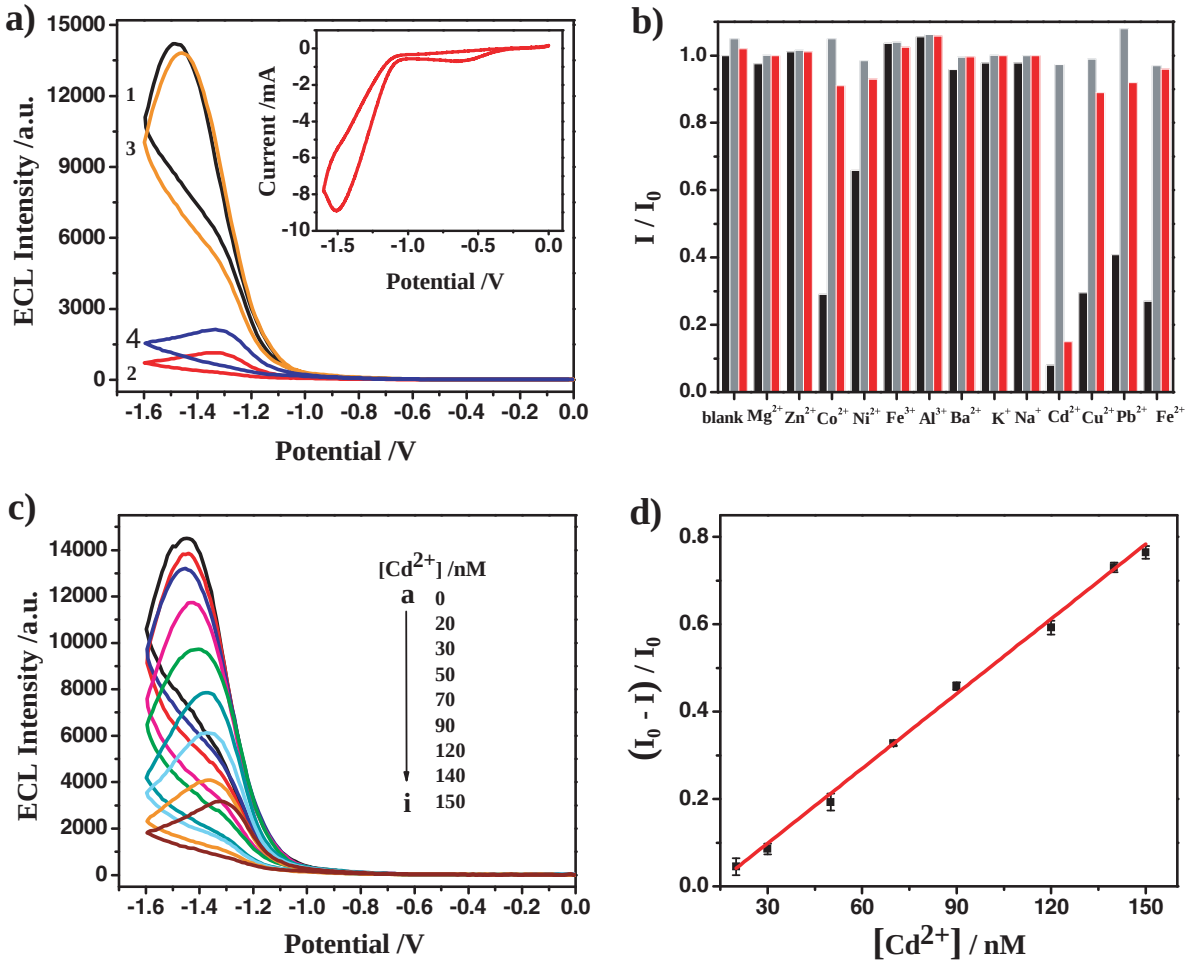

Figure 7. a) ECL-potential curves of the gGQDs (1), the gGQDs with the addition of 20 μM Cd^{2+} (2), the gGQDs with the successive addition of 20 μM Cd^{2+}, 40 μM EDTA (3), or 1 mM Cys (4) in 0.05 M, pH 7.4 TBS with 0.1 M $K_2S_2O_8$. Inset: CV corresponds to (2). b) Relative ECL intensity (I/I_0) of gGQDs (20 ppm) in the presence of various metal ions (20 μM) without any chelator (black) or with 40 μM EDTA (grey) and 1 mM Cys (red). c) ECL-potential curves of gGQDs in the presence of (a–i) 0, 20, 30, 50, 70, 90, 120, 140 and 150 nM Cd^{2+}.The electrolyte is 0.05 M, pH 7.4 TBS with 0.1 M $K_2S_2O_8$ and 1 mM Cys. d) Linear calibration plot for Cd^{2+} detection.

decrease of corresponding ECL emission. And EDTA could prevail over gGQDs and result in de-complexation of metal ion-gGQDs complex, giving rise to the recovery of ECL.

The CVs of gGQDs in the presence of Cd^{2+} was also studied (inset in Figure 7a). A strong peak at about −1.5 V appeared accompanied with increased current intensity after the addition of Cd^{2+}, which might originate from the formation of Cd^{2+}-gGQDs complex. When additional EDTA was introduced, the resulting CV resumed to the initial CV of gGQDs as shown in Figure 4a, indicating perfect de-complexation of Cd^{2+}-gGQDs complex by EDTA.

Other weak chelators were also used to compete with gGQDs for metal ions, such as glutathione, cysteamine, cysteine (Cys), tartaric acid and citric acid. Interestingly, as depicted by curve 4 in Figure 7a, and the black and red line in Figure 7b, the addition of Cys could recover the quenched ECL induced by all the metal ions (20 μM) except Cd^{2+}, which quenched the gGQDs ECL by 85% even in the presence of 1 mM Cys (50 times of Cd^{2+} concentration). Thus Cys could act as effective masking agent for the determination of Cd^{2+} with acceptable selectivity. As shown in Figure 7c, the ECL intensity of gGQDs was gradually decreased with increasing Cd^{2+} concentration in the presence of 1 mM Cys. The proposed sensor shows a linear relationship between the Cd^{2+} concentration with ECL intensity decrease over the range from 20 nM to 150 nM (R = 0.998) with a detection limit of 13 nM at signal-to-noise of 3 (Figure 7d), which is comparable with other methods such as colorimetric and fluorescence sensors.[32,33]

3. Conclusions

In summary, we developed a facile microwave-assisted approach for the preparation of stabilizer-free two-color GQDs with PL quantum yields as high as 22.9%. It was verified that reduction occurred simultaneously with the cleaving of GO

during the microwave process. ECL emission was observed from the as-prepared GQDs for the first time. The GQDs were demonstrated to possess negligible surface defect suggested by the tiny red-shift between their PL and ECL spectra. And a novel ECL sensor for Cd^{2+} was proposed based on the competitive coordination between Cys and GQDs for metal ions. This kind of ECL active GQDs are expected to have promising applications in the development of novel ECL biosensors due to their low cytotoxicity, low cost, excellent solubility, and ease of labeling.

4. Experimental Section

Chemicals and Materials: Graphite powder (KS-10, 99.95%) was obtained from Sigma–Aldrich. All other reagents were of analytical reagent grade and used without further purification. Ultrapure fresh water obtained from a Millipore water purification system (≥18MΩ, Milli-Q, Millipore) was used. 0.05 M Tris-HCl buffer solution (pH 7.4) containing 0.1 M $K_2S_2O_8$ and 0.1 M KCl was used as the electrolyte in ECL analysis.

Apparatus: The microwave synthesize of GQDs was performed on a WBFY-201 Microwave Oven equipped with atmospheric reflux device (Najing Keer Instrument Equipments Co. Ltd., Nanjing, China). The ECL intensity was detected with a Model MPI-A Electrochemiluminescence Analyzer (Xi'An Remax Electronic Science & Technology Co. Ltd., Xi'An, China). The emission window was placed in front of the photomultiplier tube (PMT) biased at 800 V. The ECL spectrum was obtained by collecting the ECL peak intensity during the cyclic potential sweep with a series of optical filters at 400, 420, 450, 470, 510, 535 and 565nm. UV-vis spectra were recorded on a UV-3600 spectrophotometer (Shimadzu, Kyoto, Japan). Photoluminescence (PL) spectra were obtained on a RF-5301PC spectrophotometer (Shimadzu, Kyoto, Japan). X-ray photoelectron spectroscopy (XPS) was carried out on an ESCALAB MK II X-ray photoelectron spectrometer. Fourier-transform infrared (FTIR) spectroscopic measurements were performed on a Bruker model VECTOR22 Fourier-transform spectrometer using KBr pressed disks. High-resolution transmission electron microscopy (HRTEM) images were taken using a JEOL 2010 electron microscope at an accelerating voltage of 200 kV. Atomic force microscopy (AFM) images were obtained on a SPI3800 controller operated in tapping mode with an acquisition frequency of 1.5 Hz and line density of 512.2 × 2 μm scans.

Synthesis of gGQDs: Graphene oxide (GO) was synthesized from natural graphite powder by a modified Hummers method.[20] Briefly, GO solution (30 mL, 0.5 mg/mL) was firstly mixed carefully with concentrated HNO_3 (8 ml) and H_2SO_4 (2 ml), thus the concentrations of HNO_3 and were H_2SO_4 were 3.2 M and 0.9 M respectively. Then the mixture was heated and refluxed under microwave irradiation for 1-5 h in microwave oven operating at a power of 240 W. The product contained brown transparent suspension and black precipitates. After cooling to room temperature, the mixture was under mild ultrasonication for few minutes, and the pH was tuned to 8 with NaOH in an ice-bath. The suspension was filtered through a 0.22 μm microporous membrane to remove the large tracts of GO and a deep yellow solution (yield ca. 33%) was separated. The mixture solution was further dialyzed in a dialysis bag (retained molecular weight: 8000–10 000 Da) and greenish yellow fluorescent GQDs were obtained (yield ca. 8%).

Synthesis of bGQDs: Prior to dialysis, the above obtained deep yellow filter solution was reduced with $NaBH_4$ (1 g) under vigorous stirring at room temperature for 1–2 h. The solution color faded to yellow. Then HNO_3 solution was added dropwise to terminate the reaction and tune the pH to 8. The suspension was filtered through a 0.22 μm microporous membrane and further dialyzed to obtain brightly blue fluorescent GQDs. For comparision, the GQDs-$NaBH_4$ mixture was also reacted at 90 °C for 1–3 h.

ECL Investigations: 0.05 M Tris-HCl buffer solution (pH 7.4) containing 0.1 M $K_2S_2O_8$ and 0.1 M KCl was used as the electrolyte in ECL analysis. The concentrations of gGQDs and bGQDs in ECL study were both 20 ppm. ECL and CV signals were obtained simultaneously via cyclic voltammetry between 0 V and –1.6 V with a configuration consisting of a gold working electrode, a platinum counter electrode, and a saturated calomel electrode (SCE) as the reference electrode. All potentials were quoted in this manuscript against this reference electrode.

Detection of Cd^{2+}: Cadmium chloride solutions with various concentration in 0.05 M Tris-HCl buffer solution (pH 7.4) were used for the determination of Cd^{2+}. To evaluate the selectivity, the quenching effects of 12 kinds of metal cations were investigated. All of the tested metal ions included: Mg^{2+}, Ba^{2+}, Co^{2+}, Fe^{2+}, Fe^{3+}, Na^{+}, K^{+}, Zn^{2+}, Al^{3+}, Cu^{2+}, Pb^{2+}, and Ni^{2+}, the counter ions were Cl^{-} or NO_3^{-}. The salt solutions were all dissolved in 0.05 M Tris-HCl buffer solution (pH 7.4).

Supporting Information

Supporting Information is available from the Wiley Online Library or from the author.

Acknowledgements

This research was financially supported by the National Natural Science Foundation of China (Nos: 50972058, 21020102038, 21121091) and National Basic Research Program of China (2011CB933502) and the International S&T Cooperation Projects of China (2010DFA42060).

Received: January 18, 2012
Revised: March 2, 2012
Published online: April 18, 2012

[1] G. Eda, Y.-Y. Lin, C. Mattevi, H. Yamaguchi, H.-A. Chen, I. S. Chen, C.-W. Chen, M. Chhowalla, *Adv. Mater.* **2010**, *22*, 505.
[2] Y. Li, Y. Hu, Y. Zhao, G. Shi, L. Deng, Y. Hou, L. Qu, *Adv. Mater.* **2011**, *23*, 776.
[3] D. Y. Pan, J. C. Zhang, Z. Li, M. H. Wu, *Adv. Mater.* **2010**, *22*, 734.
[4] K.-J. Jeon, Z. Lee, E. Pollak, L. Moreschini, A. Bostwick, C.-M. Park, R. Mendelsberg, V. Radmilovic, R. Kostecki, T. J. Richardson, E. Rotenberg, *ACS Nano* **2011**, *5*, 1042.
[5] J. Shen, Y. Zhu, C. Chen, X. Yang, C. Li, *Chem. Commun.* **2011**, *47*, 2580.
[6] S. Zhu, J. Zhang, C. Qiao, S. Tang, Y. Li, W. Yuan, B. Li, L. Tian, F. Liu, R. Hu, H. Gao, H. Wei, H. Zhang, H. Sun, B. Yang, *Chem. Commun.* **2011**, *47*, 6858.
[7] K. P. Loh, Q. Bao, G. Eda, M. Chhowalla, *Nat. Chem.* **2010**, *2*, 1015.
[8] J.-L. Chen, X.-P. Yan, *J. Mater. Chem.* **2010**, *20*, 4328.
[9] Q. S. Mei, K. Zhang, G. J. Guan, B. H. Liu, S. H. Wang, Z. P. Zhang, *Chem. Commun.* **2010**, *46*, 7319.
[10] X. Yan, X. Cui, L.-s. Li, *J. Am. Chem. Soc.* **2010**, *132*, 5944.
[11] X. Yan, X. Cui, B. Li, L.-s. Li, *Nano Lett.* **2010**, *10*, 1869.
[12] E. A. Anumol, P. Kundu, P. A. Deshpande, G. Madras, N. Ravishankar, *ACS Nano* **2011**, *5*, 8049.
[13] C.-L. Sun, C.-T. Chang, H.-H. Lee, J. Zhou, J. Wang, T.-K. Sham, W.-F. Pong, *ACS Nano* **2011**, *5*, 7788.
[14] S. Liu, F. Lu, J.-J. Zhu, *Chem. Commun.* **2011**, *47*, 2661.
[15] Y. Zhu, S. Murali, M. D. Stoller, A. Velamakanni, R. D. Piner, R. S. Ruoff, *Carbon* **2010**, *48*, 2118.
[16] W. Chen, L. Yan, P. R. Bangal, *Carbon* **2010**, *48*, 1146.

[17] Z. Ding, B. M. Quinn, S. K. Haram, L. E. Pell, B. A. Korgel, A. J. Bard, *Science* **2002**, *296*, 1293.
[18] F. R. F. Fan, S. Park, Y. W. Zhu, R. S. Ruoff, A. J. Bard, *J. Am. Chem. Soc.* **2009**, *131*, 937.
[19] L. Y. Zheng, Y. W. Chi, Y. Q. Dong, J. P. Lin, B. B. Wang, *J. Am. Chem. Soc.* **2009**, *131*, 4564.
[20] L.-L. Li, K.-P. Liu, G.-H. Yang, C.-M. Wang, J.-R. Zhang, J.-J. Zhu, *Adv. Funct. Mater.* **2011**, *21*, 869.
[21] J. Peng, W. Gao, B. K. Gupta, Z. Liu, R. Romero-Aburto, L. Ge, L. Song, L. B. Alemany, X. Zhan, G. Gao, S. A. Vithayathil, B. A. Kaipparettu, A. A. Marti, T. Hayashi, J.-J. Zhu, P. M. Ajayan, *Nano Lett.* **2012**, *12*, 844.
[22] J. L. Zhang, H. J. Yang, G. X. Shen, P. Cheng, J. Y. Zhang, S. W. Guo, *Chem. Commun.* **2010**, *46*, 1112.
[23] J. Liu, S. Fu, B. Yuan, Y. Li, Z. Deng, *J. Am. Chem. Soc.* **2010**, *132*, 7279.
[24] M.-C. Hsiao, S.-H. Liao, M.-Y. Yen, P.-I. Liu, N.-W. Pu, C.-A. Wang, C.-C. M. Ma, *ACS Appl. Mater. Interfaces* **2010**, *2*, 3092.
[25] C. Mattevi, G. Eda, S. Agnoli, S. Miller, K. A. Mkhoyan, O. Celik, D. Mastrogiovanni, G. Granozzi, E. Garfunkel, M. Chhowalla, *Adv. Funct. Mater.* **2009**, *19*, 2577.
[26] S. C. Ray, A. Saha, N. R. Jana, R. Sarkar, *J. Phys. Chem. C* **2009**, *113*, 18546.
[27] Y. Li, Y. Zhao, H. Cheng, Y. Hu, G. Shi, L. Dai, L. Qu, *J. Am. Chem. Soc.* **2012**, *134*, 15.
[28] H. Li, X. He, Z. Kang, H. Huang, Y. Liu, J. Liu, S. Lian, C. H. A. Tsang, X. Yang, S.-T. Lee, *Angew. Chem.* **2010**, *122*, 4532.
[29] N. Myung, Y. Bae, A. J. Bard, *Nano Lett.* **2003**, *3*, 1053.
[30] Y. Q. Dong, N. N. Zhou, X. M. Lin, J. P. Lin, Y. W. Chi, G. N. Chen, *Chem. Mater.* **2010**, *22*, 5895.
[31] Y. Bae, D. C. Lee, E. V. Rhogojina, D. C. Jurbergs, B. A. Korgel, A. J. Bard, *Nanotechnology* **2006**, *17*, 3791.
[32] Y. Xue, H. Zhao, Z. Wu, X. Li, Y. He, Z. Yuan, *Analyst* **2011**, *136*, 3725.
[33] Y. Wang, X. Hu, L. Wang, Z. Shang, J. Chao, W. Jin, *Sens. Actuators B* **2011**, *156*, 126.
[34] W. Hao, A. McBride, S. McBride, J. P. Gao, Z. Y. Wang, *J. Mater. Chem.* **2011**, *21*, 1040.
[35] F. Jalilehvand, B. O. Leung, V. Mah, *Inorg. Chem.* **2009**, *48*, 5758.
[36] Y.-H. Chan, Y. Jin, C. Wu, D. T. Chiu, *Chem. Commun.* **2011**, *47*, 2820.